AIIM

Association for Information and Image Management
1100 Wayne Avenue, Suite 1100
Silver Spring, Maryland 20910
301/587-8202

Centimeter

Inches

MANUFACTURED TO AIIM STANDARDS
BY APPLIED IMAGE, INC.

1 of 1

Conf-930726--1

THE APPLICATION OF NONDESTRUCTIVE TECHNIQUES TO THE TESTING OF A WIND TURBINE BLADE

Herbert J. Sutherland
Sandia National Laboratories
Albuquerque, NM 87107

and

Walt Musial
National Renewable Energy Laboratory
Golden, CO 80401

ABSTRACT

NonDestructive Testing (NDT) is commonly used to monitor structures before, during and after testing. This paper reports on the use of two NDT techniques to monitor the behavior of a typical wind turbine blade during a quasi-static test-to-failure. The test used a three-point spanwise load distribution to load a 7.9-m blade to failure. The two NDT techniques used were acoustic emission and coherent optical. The former monitors the acoustic energy produced by the blade as it is loaded. The latter uses electronic shearography to measure the differences in surface displacements between two load states with an accuracy of a few microns. Typical results are presented to demonstrate the ability of these two techniques to locate and monitor both high damage regions and flaws in the blade structure. Further, this experiment highlights the limitations in the techniques that must be addressed before one or both can be transferred, with a high probability of success, to the inspection and monitoring of turbine blades during the manufacturing process and under normal operating conditions.

INTRODUCTION

NonDestructive Testing (NDT) is a powerful tool for reducing costs, for improving and maintaining product quality and for the inspection of in-service components. The use of NDT techniques, also called NonDestructive Evaluation (NDE), is common in a number of industries, especially the aircraft industry, for quality control (QC) and quality assurance (QA). However, NDT for the inspection and testing of wind turbines has not been used widely. One notable exception is the QA/QC program adopted by Gougeon Brothers. They have used acoustic waves to inspect and control the quality of the wood veneer used in the construction of their wind turbine blades. The primary reason NDT techniques have limited use in the wind turbine industry is that suitable test systems and procedures suited to the inspection of wind turbine components have not been demonstrated to be cost effective and reliable.

In a "proof-of-concept" experimental program, two NDT systems, acoustic emission [1] and coherent optical [2], were used to monitor the quasi-static test to failure of a 7.9-m wind turbine blade. It was loaded at three points with a load distribution that simulated the load distribution on the blade under field operation. These two techniques were chosen for this study because they have a high potential for use as QA/QC tools in manufacturing and for in-service inspection of wind turbine blades.

The acoustic emission (AE) system used 23 sensors located in two arrays on the blade. Data from the sensors were processed in real time giving both the location and a measure of the degree of damage. The data were also recorded on the hard disc to allow post-test processing for more extensive analysis.

The coherent optical technique used electronic shearography. The system measures differences in surface displacements between two load states with an accuracy of a few microns. Two loading systems were used here. For pre- and post-test inspection, the blade was loaded thermally over relatively small areas. During the course of the experiment, the structural loads, applied through the whiffle tree were used. The system was able to locate "flaws" and internal structure in the blade. For the pre-test inspection, the location of flaws and internal structure were marked on the blade. An approximately 0.6-m (2-ft) square, near the root of the blade, was monitored during the course of the test. The post-test inspection examined previously identified flaws and the failed portions of the blade.

This paper presents the details of this proof-of-concept experiment and discusses the applicability of acoustic emission and coherent optical NDT techniques to the inspection of wind turbine blades during a quasi-static test to failure. A complete description of the experiments, procedures and test results are provided in Ref. 3.

THE QUASI-STATIC BLADE TEST

The quasi-static blade test was conducted on a 7.9-m blade, see Fig. 1, in the NREL full-blade test facility [4]. The blade was designed using the NREL thin airfoil family [5]. It was fabricated at Phoenix Industries to demonstrate the performance of the NREL thin-airfoil series [6]. The blade was constructed primarily of fiberglass reinforced polyester with a total weight of 287 kg (633 lb).

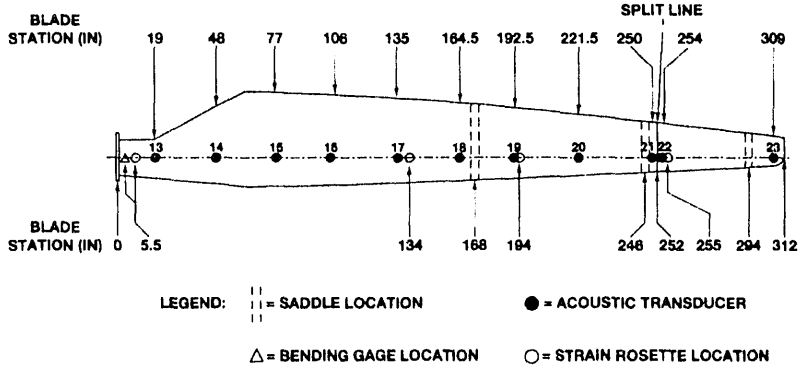

Figure 1. Schematic Diagram of the 7.9 Meter Blade.

Blade Loads

The blade was loaded during this experiment using a three-point spanwise load distribution. Loads were applied to the blade with saddles made from laminated plywood. Saddles were fit to the blade at each load point and were padded with neoprene to distribute the load. Loads were transferred to the blade saddles using a single point load through a series of spanner beams and compliant links, called a whiffle tree. A gantry crane, equipped with a hydraulic winch, was used to apply the single, point load from above [4].

Figure 2 shows the bending moment distribution used to load the blade for this experiment. This figure shows that the three-point load is a good approximation of the ten point triangular distribution used at North Dakota State University in a previous quasi-static test to failure of this blade. The saddle locations used to achieve this load distribution were at stations 168, 246, and 294; i.e., 427, 625 and 1588 cm (168, 246 and 294 in) from the root-end of the blade.

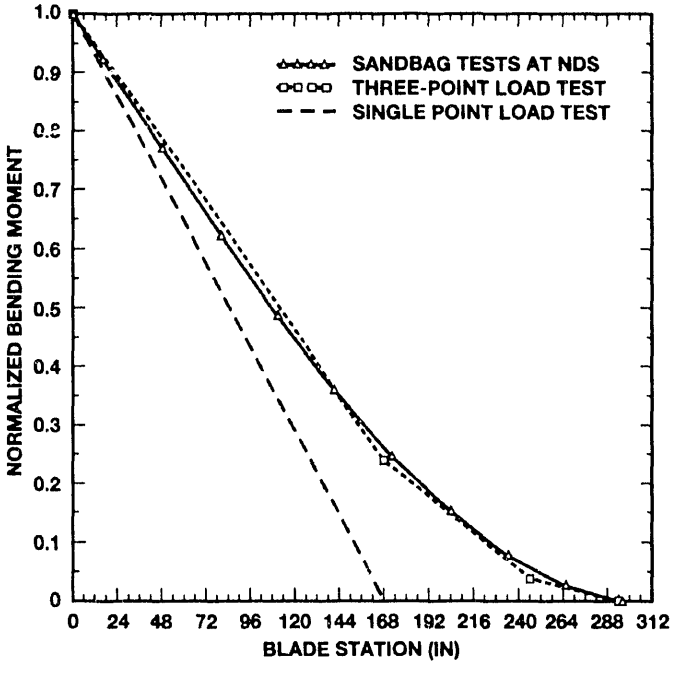

Figure 2. Load Distribution on the 7.9 Meter Blade.

The deflection of the blade and strains in the skin of the blade were measured during the course of the experiment, see Fig. 1. The deflections were measured at the three load saddles. The strain gages were three-element rectangular rosettes placed on the tension (bottom) side of the blade at

stations 15.5, 134, 194 and 255; (39, 340, 493, and 648 cm). A half-bridge bending gage was used at station 5.5 (14 cm) also.

Test Procedure

During the test, the blade was loaded in increments of 4.5 kN (1000 lb). Strain gage data were recorded continuously at a 20-Hz sampling rate. Deflection measurements were taken manually at each 4.5-kN load interval. When 8.9 kN (2000 lb) was reached, the load intervals were reduced to 2.2-kN (500 lb) increments until failure occurred. After failure, the blade was unloaded and the failure locations were documented using a video camera. Additional testing was conducted on the blade after the initial failure. Those results are reported in Ref. 3.

Test Results

The three-point loading test resulted in a failure of the blade at approximately 30.54 cm (12 in) inboard from the split line of the pitchable tip at station 240 (609.6 cm) , 6 inches inboard from the middle saddle. The failure occurred near the point where the internal spar (shear web) was terminated and the pitch shaft transitions to a smaller diameter shaft. The peak load at failure was recorded at 17.46 kN (3925 lb). This load results in a root failure load of 97.9 kN-m (72,528 ft-lb). The bending moment at the failure location was 4.85 kN-m (3596 ft-lb). The failure appeared as a chordwise crease in the skin on the compression surface.

Typical strain measurements for station 134 are shown in Fig. 3. Stations 134 and 194 had the highest strains in the blade, see Ref. 3. Strains at these locations were over an order of magnitude higher than the root strains. Strains at station 255 were in the same range as the root strains.

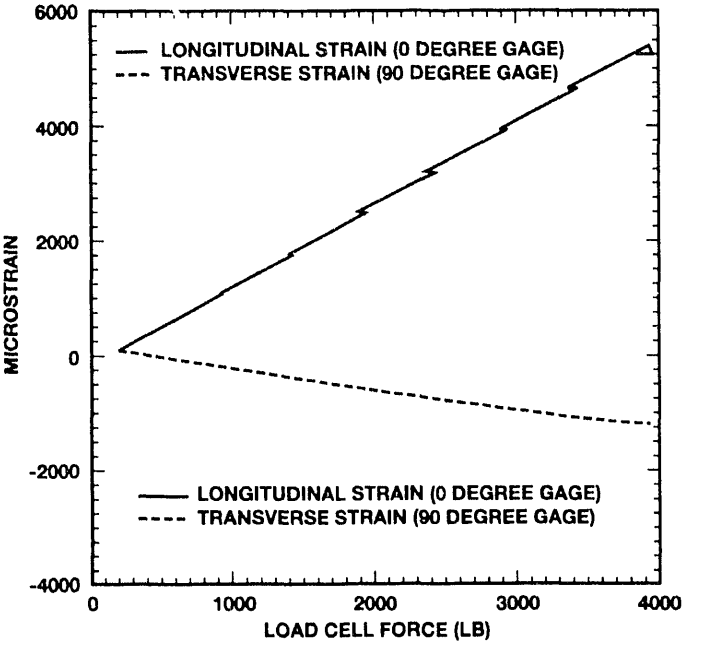

Figure 3. Blade Skin Strains at Station 134.

Post-Test Inspection

The primary failure of the blade occurred at station 240 where the steel pitch shaft of the tip spoiler mechanism was bent inboard of the cam mechanism as a result of the loading applied during the first part of the test. The skin was also buckled on the low-pressure side of the blade in the same radial location as the failure of the steel tip mechanism itself.

THE ACOUSTIC EMISSION TECHNIQUE

Acoustic emissions are acoustic waves generated by a material when it undergoes inelastic strain or rupture [1]. In the case of fiberglass, there are three main sources of emission. These are a) matrix cracking, b) fiber fracture and c) fracture of the fiber-matrix interface. A tear in the fiberglass will involve all three mechanisms. Which of the mechanisms will generate emission at a point in a test will depend upon the material characteristics and the local stress field in every region of the material. The presence of acoustic emissions in a fiberglass structure subjected to an external load indicates a local failure in some part of the structure. During the initial loading or at loads that are low when compared to the design load, fiberglass often generates some acoustic emissions. These emissions often do not signify significant flaws but are the product of regions with high residual stresses; e.g., an overly tight wrap in a wrapped fiberglass vessel.

In a large fiberglass structure, the optimum use of acoustic emission testing involves locating spatially the sources of acoustic emissions. One common way for locating sources is to determine the arrival time of an individual emission burst at different sensors. The location is then determined by triangulation. The main problem with source location in fiberglass

is that the AE events are attenuated very quickly. At moderate acoustic emission frequencies, the determination of a source location in two-dimensions can require a prohibitively large number of sensors.

Experimental Design and Setup

For this experiment, a 24-channel AE system was used. Twelve (12) sensors were placed in an array covering the root of the blade and 11 were located along the length of the rest of the blade, see Fig. 1. This configuration permits an examination of the whole surface of the root region of the blade but limits the system to determining the location of the emission sources on the rest of the blade to their spanwise station (linear distance from the root). For each emission, the following parameters were recorded to disk: the time of arrival at the sensor (to the nearest 0.125 microsecond), the number of the sensor "hit" (excited by the emission), the signal rise time, the load applied to the blade, the AE count, the signal duration, the signal strength and the signal peak amplitude. The system was set to ignore signals with under three AE counts or a duration of less than 100 microseconds. Signals with one or two counts are often random noise, and signals under 100 microseconds are usually electromagnetic, not acoustic, in origin.

During the test, the location of AE events were plotted to provide real-time damage detection. Additional analyses of the data were performed after the test was completed.

Real-Time Test Results

Figure 4a shows a plot of the location of AE emission for the root of the blade during the course of the experiment. In this figure, the circumferential distance around the root has been "unfolded" into a linear plot. The break line for this plot is at circumferential station 0 which is coincident with approximately circumferential station 60. Transducers 1 and 9 are on the compression side (top) of the blade and transducer 3 and 11 are on the tension side (bottom) of the blade. The other transducers are placed about the circumference of the root as shown in Fig. 4a. As can be seen in this plot, most of the emissions came from the compression side (top) of the blade, between transducers 9 and 12. The events were located primarily between blade stations 12 to 20. Figure 4b shows a similar plot along the span of the blade. This figure is the linear location plot for the blade region. There was a small cluster of events between stations 40 and 55, near sensor 14. Most of the events were from a region near station 240 (between sensors 20 and 21).

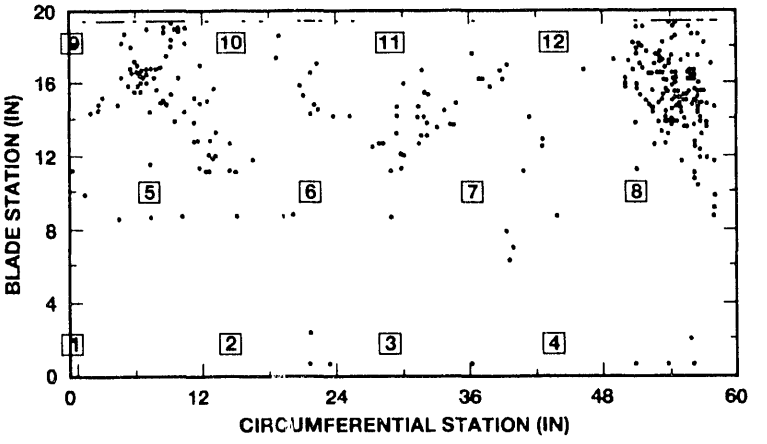

4a. Around the Circumference of the Root

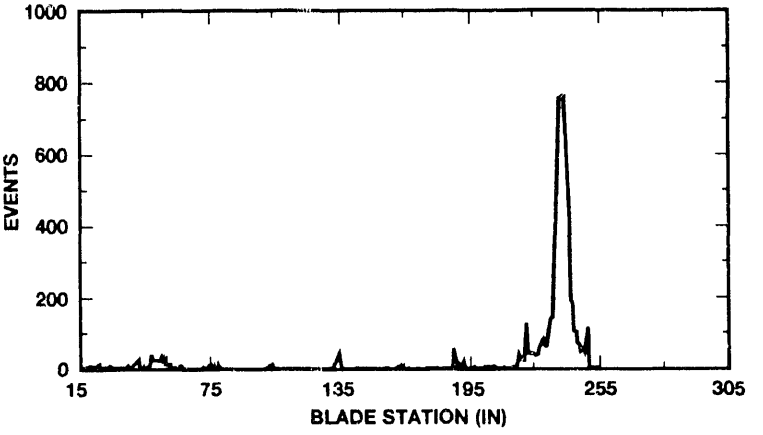

4b. Along the Span of the Blade.

Figure 4. Acoustic Emission Events as a Function of Position.

Figure 5a shows the AE events in the root of the blade plotted as a function of the load on the blade. In this plot, the number of AE events for transducer 1 through 12 are summed together to get the total number of events emanating from the root of the blade. The large number of events noted in this figure implies that significant damage may be accumulating in the root of the blade. However, the location graph, Fig. 4a, illustrates that the damage is wide spread and not concentrated into a few serious flaws. Figure 5b shows the events versus load curve along the span of the blade; i.e., the AE events from

transducers 13 through 23 are summed together. This plot indicates that the on-set of failure started at about 12.9 kN (2900 lb) load. Fig. 4b illustrates that these AE events are clustered at or near the blade failure zone between stations 240 and 250.

Post-Test Analysis

In the root of the blade, Fig. 4a, about 460 events were located during the loading. Most of the events were in the band between stations 12 and 20. In this band there is a concentration of events on the upper (compression) side of the blade and toward the leading edge; i.e., from transducer 9 towards transducer 12. The root region continued to emit on subsequent loading up to 36.9 kN (8300 lb) but did not fail, see Ref. 3. Examination of a post-test section from this region showed cracks in the epoxy running parallel to the fibers but no obvious sign of fiber damage.

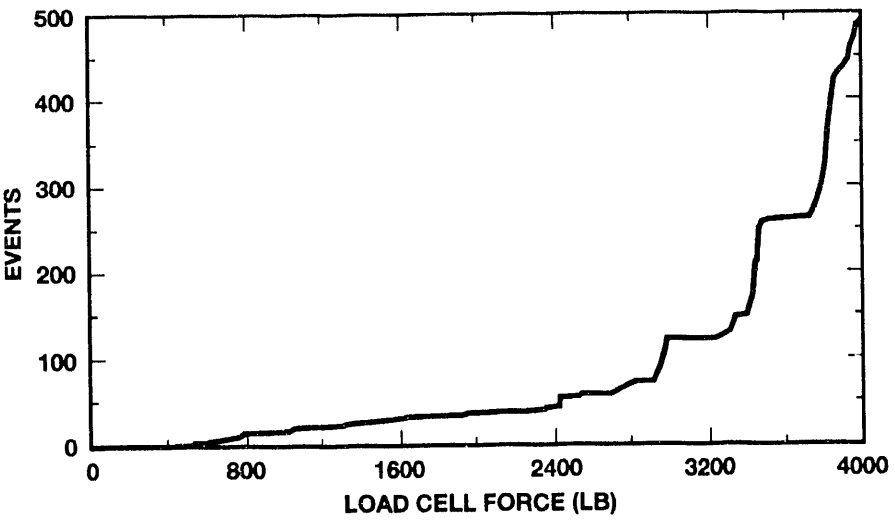

5a. Around the Circumference of the Root.

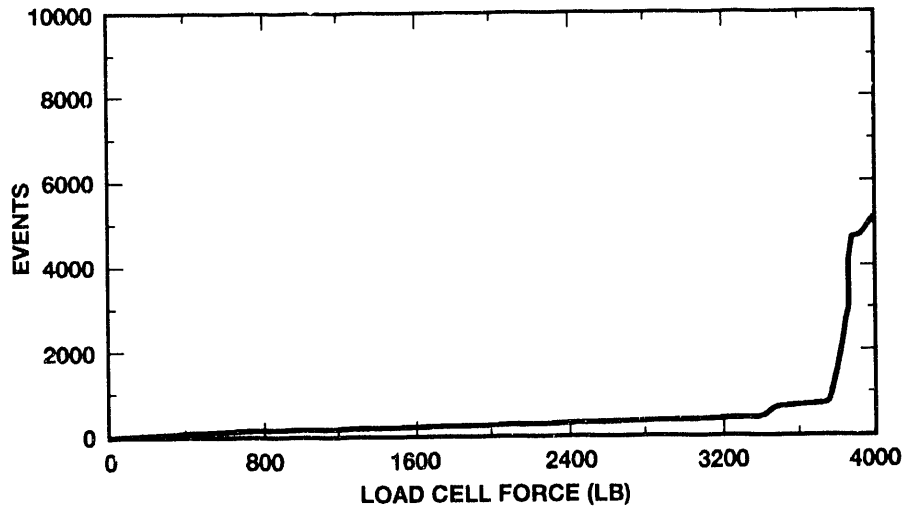

5b. Along the Span of the Blade.

Figure 5. Acoustic Emission Events as a Function of Load.

The region from station 40 to station 55 showed a clustering of events, see Fig. 4b. Appreciable emissions started at a load of 10.7 kN (2400 lb) and remained at a relatively constant rate with increasing load, see Fig. 5b. In the initial loading of the blade, the AE activity occurred primarily as the load on the blade increased. During periods where the load was held constant, there was little AE activity. This is a sign of "stable" damage accumulation, i.e., flaws are growing only under an increasing load. In the subsequent blade tests to 36.9 kN (8300 lb), the emitting structure between stations 40 and 56 started to accumulate damage during both increasing and constant loads, see Ref. 3. The structure reached a point where almost all of the possible damage had occurred but the rest of the blade was still capable of bearing the load. Sectioning of the blade showed that the rear side of the box spar had debonded from the top skin in the region from station 37, where it started, to approximately station 50. Also found was a section of the skin on the compression side (top) of the blade, approximately 12.7 cm (5 in) wide and running from station 37 to station 54, which was only about one half the thickness of the rest of the skin in this area. It is possible that this thinned skin underwent buckling and produced some of these emissions.

The AE events for stations 234 to 242 started at approximately 12.4 kN (2800 lb). Appreciable emissions indicated that failure started at approximately 15.1 kN (3400 lb) and continued to the ultimate load of 17.46 kN (3925 lb). The post-test examination of the sectioned blade showed that the spar was debonded from the compression side (top) from about station

230 to the end of the spar at about station 239. There was also buckling and tearing of the top skin between 236 and 242 inches. This failure zone is exactly the region of failure located by AE.

Discussion

The acoustic emission test clearly detected the primary blade failure near station 240 and showed that there was little damage in this region until the load exceeded 15.1 kN (3400 lb). The debonding of the rear spar near station 37 was seen to start at a load of 10.7 kN (2400 lb). The debond propagated outward as the load was increased until it finally stopped around station 56. This damage did not have a significant effect during these overload tests but may have lead to a long term fatigue failure in actual service.

The real time data observed the build up of damage at the locations well before blade failure. Thus, AE can be used to detect "hot spots" or "weak points" in the structure before they fail. For the failure at station 240, the AE events marked this area at a load of 15.1 kN (3400 lb) or approximately 95 percent of the ultimate load. For station 37, the area was located at a 10.7 kN (2400 lb) load or approximately 67 percent of the ultimate load. In both cases, the blade could have been unloaded before catastrophic failure occurred.

COHERENT OPTICAL

Technique Description

The measurement category of "coherent optics" covers a broad range of interferometric techniques including single-point interferometry, holographic interferometry (holometry), electronic speckle pattern interferometry (ESPI) and shearography [3]. All of these techniques use the wavelength of light as a base metric, and an interference geometry of some sort to make the actual measurement. In other words, in all these techniques, light is bounced or scattered off an object of interest. As the object moves, the distance the light travels (the optical path) changes, and modifies the phase of the scattered light. This light is then combined with another light beam of the same wavelength (a reference or undisturbed beam) to produce optical interference, which converts the optical phase into intensity variations, which can be measured. Holometry, ESPI, and shearography are all "wide area" imaging techniques, where the interference is manifested as dark fringes superimposed on an image of the object under test. Typical sensitivity to surface displacement is a few microns.

The technique used for this test was shearography. In shearography, the reference beam is derived from the object, by "shearing" the image; i.e., the interference image is produced by two images that are slightly shifted relative to one another. This results in interferometrically comparing motion at two nearby points, which actually gives a measurement of surface slope. The major advantage of shearography over the other configurations is its tolerance of object motion. Since the test and reference beams follow nearly common paths, their combination is insensitive to fairly large motions of the test object relative to the optical system, while still able to detect local anomalies or deformations. While holometry and ESPI require careful vibration isolation, shearography is much more suitable for a field test such as this one. One disadvantage of shearography is that quantitative displacement analysis is somewhat more difficult than in ESPI or holometry. The major use of shearography has been in flaw *localization* as opposed to quantitative displacement analysis, and that was how it was used for this experiment.

Experimental Setup

The system used here was the United Technologies Pratt & Whitney (P&W) electronic holography/shearography inspection system (EHIS/ESIS). This is an "open" system, capable of being configured for either ESPI or shearography. The particular system consisted of an optical head supported by a tripod, and a separate rack of electronics containing the digital image processor, computer, video display and hard copy and other support electronics.

For the pre-test analysis, the compression (top) side of the blade was inspected at 0.3 m (1 ft) increments, using a heat gun to thermally stress the blade. Thermal stressing was chosen for the pre-test inspection for its combination of convenience and sensitivity to debonds and delaminations, which were assumed to be the most likely flaws in the blade. These flaws have both a lower thermal conductivity and lower mechanical stiffness, so under thermal stress the debonded area tends to

bulge out from the surrounding surface. Laboratory tests of debond detection in similar composite structures with thermal stress indicate a sensitivity to flaws of approximately 2.5 cm (1 in) in diameter.

The primary data output of this system is a live video image of the interference fringes. By either allowing the part under test to move slowly (in this case by cooling), or by introducing an intentional phase shift in one of the optical beams, fringes can be observed moving over the area of interest. This fringe motion makes flaws and discontinuities much more visible than they are in static photographs of the fringe fields (Ref. 3). Three methods of recording data were used: video hard copy of fringe images, a videotape of the moving fringe images, and marking suspect areas on the blade surface while viewing the live fringes. The latter method is the easiest to relate to the actual blade geometry and is the primary method used to relate the shearography results to the post-mortem dissection of the blade. A digital image archive would have been desirable. This would have allowed the static interferograms to be processed for best display, rather than relying on the video hard copy for archiving the data.

Pre-Test Results

For the pre-test inspection, 39 views were taken of the blade compression (top) surface. These views of the skin concentrated on the sections of the blade where the main spar or other underlying structures reinforced the skin. Another 16 views were used to inspect the entire surface of the blade root.

Very few obvious flaws were detected on this blade by coherent optics. Various subsurface structure such as the spar webs and lamination thickness changes were readily visible. Several anomalous areas, as well as the apparent substructure, were marked on the blade for possible post-test examination. One of the anomalous areas, between stations 36 and 48, over the spar, was selected for observation during the test.

Real-Time Test Results

During the blade fracture test, the above mentioned area near the blade root was monitored with the shearography system. The optical head was arranged to look down on this section of the blade. While the blade was being subjected to the large forces and deflections necessary to stress it to failure, skin deformations rapidly exceeded the measurement range of shearography. At each load interval, a change of about 10 pounds (the whiffle tree single point load) gave a reasonable number of fringes. Although some change in character of the deformation was observed, no obvious flaws or breakage appeared during the test in the area under observation.

Post-Test Results

The area between stations 36 to 48, over the spar, was inspected after the test, again using thermal stress. It appeared that the anomaly grew during the test. The post-mortem of this area showed a debonding of the spar and the skin (also discussed above). The original indication of a suspected "problem" in this area can be attributed to a thinning of blade skin. Shearography indicated that the deformation of this section was significantly different from its surroundings. The post-mortem was required to determine that the difference was attributable to a thin skin.

Several small flaws were noted and marked on the blade skin during the pre-test examination. Two flaws, near the transition from the circular root to an airfoil blade section, had significant AE activity during the blade loading. Post-test shearographic inspection of this area using thermal stress revealed that the two flaws had grown in size. Both flaws appeared to be small (approximately 35 cm in diameter), near-surface delaminations, and probably were not structurally significant. A post-mortem examination of one of the flaws showed that it was a region of high porosity (a manufacturing "bubble") near the surface of the blade. Under microscopic examination, the flaw showed evidence that it had grown (approximately doubling in size) during the course of the experiment.

After the blade failed, there was clearly a delamination between the spar and the skin in the area of failure. This area was examined with shearography, again using thermal stress, to determine how well shearography could locate the end of the debonded area. The shearographic image indicated a discontinuity starting at about station 224.

Discussion

As mentioned under technique description, coherent optical techniques are sensitive to surface motion, and hence to environmental factors such as acoustic vibrations or temperature variations. In this test, shearography was used since it is more robust against these disturbances than is ESPI. For the pre-test inspection, partial coverage of one side of the blade and the root (55 views total) took almost two days, including equipment setup. The testing was slowed by equipment problems: the laser was unstable (probably due to temperature) and quite a bit of time was spent waiting for it to settle. Without this problem, the area tested could perhaps have been covered in a single day. In any case, significant time was spent moving equipment, re-positioning the associated test hardware to allow a clear view, etc. During the static test itself, the coherent optical inspection followed the test in real time, and little if any delay was added for data taking. However, only one small portion of the blade could be monitored.

Despite the problems discussed here, the shearography technique was able to locate manufacturing flaws (areas of high porosity), relatively thin skin sections, structural supports (as with the spar) and structural discontinuities (at the end of the spar).

CONCLUDING REMARKS

The results given here strongly support the use of acoustic emission in both evaluating blade design and in proof testing blades after their manufacture. This technique followed the initial failure of the blade in real time and was able to locate other areas where damage was accumulating. Additional tests on this blade verified these active AE areas as potential failure zones. Although the coherent optical test results were highly encouraging, the use of this technique is currently best limited to QA procedures rather than to field inspections. In a dedicated installation, with proper handling equipment and fixturing for the blade, many of the aforementioned environmental stability problems can be solved. Also, with proper handling and mounting for the optical equipment, it would be possible to do a complete surface inspection in a few hours. This technique has been demonstrated in a production environment in the aerospace industry.

ACKNOWLEDGMENTS

The research cited here was done by a team that included, in addition to the authors, Alan G. Beattie and Bruce D. Hansche of Sandia National Laboratories, Jack Allread and Jim Johnson of the National Renewable Energy Laboratory, and Mike Summers of United Technologies (Pratt & Whitney). Alan was responsible for the acoustic emissions, Bruce and Mike for the coherent optical, and Jack and Jim for the blade test. The authors gratefully acknowledge the significant contributions made by team members to the research cited here.

This work is supported by the U.S. Department of Energy under contract DE-AC04-76DP00789 and contract DE-AC02-83CH10093.

Bibliography

1. Beattie, A. G., "Acoustic Emission, Principles and Instrumentation," J. of Acoustic Emission, Vol. 2, Number 1/2, 1983, p. 95.
2. Vest, C. M., Holographic Interferometry, John Wiley & Sons, New York, 1979.
3. Sutherland, H. J., et al, The Application of Non-Destructive Techniques to the Testing of a Wind Turbine Blade, SAND93-1380, Sandia National Laboratories, Albuquerque, NM, 87197, in publication.
4. Musial, W., and Allread, J., "Test Methodology and Control of Full-Scale Fatigue Tests on Wind Turbine Blades," Wind Energy-1993, ASME, SED-Vol. 14, p. 199.
5. Tangler, J. L. , and Somers, D. M., "Status of the Special Purpose Airfoil Families," Proceedings of Windpower '87, San Francisco, October 1987, p. 99.
6. Tangler J., Smith B., Jager D., McKenna E., and Allread J., "Atmospheric Performance Testing of the Special-Purpose SERI Thin Airfoil Family: Preliminary Results", Proceedings of Windpower '89, San Francisco, September 1989, p. 115.

DATE
FILMED
9/20/93
END